Bull. Mater. Sci., Vol. 40, No. 4, August 2017, pp. 683–690
DOI 10.1007/s12034-017-1426-9

In situ synthesis and properties of self-reinforced Si_3N_4–SiO_2–Al_2O_3–Y_2O_3 (La_2O_3) glass–ceramic composites

ZHIWEI LUO*, ANXIAN LU, LEI HAN and JUN SONG
School of Materials Science and Engineering, Central South University, Changsha 410083, PR China
*Author for correspondence (loaswell@163.com)

MS received 14 April 2016; accepted 24 October 2016; published online 26 July 2017

Abstract. *In-situ*-grown β-Si_3N_4-reinforced SiO_2–Al_2O_3–Y_2O_3 (La_2O_3) self-reinforced glass–ceramic composites were obtained without any β-Si_3N_4 seed crystal. These composites with different compositions were prepared in a nitrogen atmosphere for comparison of phase transformation and mechanical properties. The results showed that SiO_2–Al_2O_3–Y_2O_3 (La_2O_3) glass can effectively promote α- to β-Si_3N_4 phase transformation. The crystallized $Y_2Si_2O_7$–$La_{4.67}Si_3O_{13}$ phases with a high melting point significantly benefited the high-temperature mechanical properties of the composites. The Si_3N_4–SiO_2–Al_2O_3–Y_2O_3 (La_2O_3) glass–ceramic composites exhibit excellent mechanical properties compared with unreinforced glass–ceramic matrix, which is undoubtedly attributed to the elongated β-Si_3N_4 grains. These glass–ceramic Si_3N_4 composites with excellent comprehensive properties might be a promising material for high-temperature applications.

Keywords. Crystallization; glass–ceramics; phase transformations; silicon nitride.

1. Introduction

In the late 1980s, the number of reports of rare-earth (RE) aluminosilicate glasses began to increase, as it was realized that they exhibit favourable chemical, mechanical and optical properties, which exhibit many potential technological applications, e.g., as laser ion hosts, optical lenses, sealing glass, as *in vivo* radiation delivery vehicles and storage matrices for radioactive waste [1–4]. Furthermore, RE–Si–O–N and RE–Si–Al–O–N glasses have since been prepared in systems, and some evidence shows that, as the rare-earth oxides content increases, Young's modulus, microhardness, bending strength, fracture toughness, glass transition temperature and viscosity increase with increases in cationic field strength (CFS) [5–9]. As is known to all, crystallization heat treatments on oxynitride glasses can lead to significant improvements in mechanical properties such as elastic modulus, microhardness, bending strength and fracture toughness. So far, as we know, however, there are only a few previous investigations on crystallization of RE-containing oxynitride glasses [10–13]. For example, Liddell and Thompson showed that the mixed α-$Y_{1.5}La_{0.5}Si_2O_7$ should be stable before any transformation occurs in a mixed Y–La–Si–Al–O–N glass [14]. It seems that the crystallization of nitrogen-containing phase from the oxynitride glasses is very difficult. Thus, most of the content of nitrogen generally remains in the residual glass phase. As per our knowledge, the crystallization of β-Si_3N_4 from silicate oxynitride glasses after heat treatment has been reported only by Satet and Hoffmann [10], in which systematic investigations of the Ostwald ripening behaviour of β-silicon nitride grains dispersed in Me–Mg–Si–O–N glasses had brought some insights on the impact of Me^{3+} cations (Me = La, Lu, Sc, Sm, Y, Yb) on grain growth anisotropy of β-Si_3N_4.

On the other hand, due to the excellent combination of thermo-mechanical properties, Si_3N_4 ceramic is widely applied to several industrial fields [15–20]. The intrinsically brittle nature of ceramic is a critical issue, but can be overcome by introducing whisker-like microstructural features. Meanwhile, recent literatures have concentrated on Si_3N_4-reinforced glass–ceramic matrix composites due to their good chemical erosion resistance, oxidation resistance, thermal-shock resistance and mechanical properties, and the resultant glass–ceramic Si_3N_4 composites exhibited an attractive combination of excellent comprehensive performances [21–25]. These research results revealed that obtaining a bimodal microstructure, i.e., abnormally grown Si_3N_4 grains surrounded by fine glass–ceramic matrix, is an effective method to further improve strength and fracture toughness. So far, as we know, rare-earth aluminosilicate glasses have been found useful to promote liquid-phase sintering of silicon-carbide-based ceramics [26–28]. In these systems, an oxide powder mixture based on SiO_2–Al_2O_3–RE_2O_3 system forms a liquid at high temperatures. Similarly, synthesis of dense Si_3N_4 ceramic usually requires the use of additives, which react with the SiO_2 present on the Si_3N_4 surface to form a liquid phase.

Intrinsically, pure SiO_2–Al_2O_3–RE_2O_3 glass–ceramic exhibits relatively low mechanical properties, which limit their use in many structural applications. The disilicates $La_2Si_2O_7$ and $Y_2Si_2O_7$ show a non-congruent melting behaviour at 1750 and 1775°C, respectively. $Y_2Si_2O_7$–$La_2Si_2O_7$ can be used in severe environments with high temperature

water vapour corrosion and fast cooling–heating cycle owning to its good damage tolerance and low CTE [29]. Obviously, during the sintering process, the SiO_2–Al_2O_3–RE_2O_3 system glass could form a liquid phase at a lower temperature, which subsequently is crystallized into a compound with a high melting point. As is known to all, the mixture of rare earth oxides (Y_2O_3 and La_2O_3) is readily available and not expensive. Moreover, Lange *et al* [30] have shown that in the Si_3N_4–SiO_2–Y_2O_3 system, $Y_2Si_2O_7$ is the most oxidation-resistant secondary phase for Si_3N_4 ceramic because it is the only Y-containing phase in equilibrium with SiO_2, the oxidation product of Si_3N_4.

The purpose of this study is to evaluate the mechanical properties of the *in-situ*-grown Si_3N_4–rare-earth aluminosilicate self-reinforced glass–ceramic composites without any β-Si_3N_4 seed crystal at relatively low temperatures. The size and morphology of β-Si_3N_4 grains via a dissolution–reprecipitation mechanism from α-Si_3N_4 were also investigated by scanning electron microscopy (SEM) and high-resolution transmission electron microscopy (HR-TEM).

2. Materials and methods

2.1 *Preparation of materials*

The composition of the rare-earth aluminosilicate glasses (shown in table 1) consists of 24 mol% Y_2O_3 (or La_2O_3), 16 mol% Al_2O_3 and 60 mol% SiO_2. The respective glasses were named GY# and GL#, respectively. High-purity rare-earth oxides La_2O_3 (purity $\geq$ 99.999%) and Y_2O_3 (purity $\geq$ 99.999%), analytical grade Al_2O_3 (purity $\geq$ 99.99%) and SiO_2 (purity $\geq$ 99.99%) were mixed in water-free ethanol using an agate ball as the milling medium for 10 h. The powder mixtures were dried after their grinding. A 100 g portion of powder was melted in a crucible kept in an electrically heated furnace at 1550°C for 2 h in air. The melt was poured into deionized water to form a glass frit. The glass frit samples GY# and GL# were also milled by agate balls for 10 h.

Table 1. Composition of the RE_2O_3–Al_2O_3–SiO_2 (RE = Y, La) glasses.

	Composition (mol%)			
Sample	Y_2O_3	La_2O_3	SiO_2	Al_2O_3
GY#	24.00	0	60.00	16.00
GL#	0	24.00	60.00	16.00

The raw materials used in this study were glass–ceramic Si_3N_4 composites with different glass frit contents. The compositions of the investigated glass–Si_3N_4 composites are listed in table 2. α-Si_3N_4 (purity $\geq$ 99.9%) starting powders and glass frit (GY# and GL#) were mixed in the appropriate proportion in water-free ethanol using an agate ball as the milling medium for 24 h. The powder mixtures were dried and sifted through a 200 mesh screen. The mixed powders were uniaxially pressed in a steel mould of Φ 40 mm at a pressure of 300 MPa. The specimens were taken in a graphite crucible. A two-step sintering process was carried out in a graphite resistance furnace and a nitrogen atmosphere (purity 99.99%). The samples were first heated to 1100°C at a rate of 10°C min^{-1} and held there for 2 h; then they were further heated to 1650°C at a rate of 20°C min^{-1} and held there for 4 h in 0.15 MPa of high-purity nitrogen atmosphere; the cooling process was accomplished by switching off the power.

2.2 *Characterization techniques*

A differential scanning calorimeter (DSC, Netzsch 404 PC) was used to obtain thermal curves of glass frit (samples GY# and GL#). Phase identification was investigated using an X-ray diffractometer (D/max 2500 model) with Cu-K_α radiation using an incident wavelength of 0.154 nm. Voltage and current were selected as 40 kV and 50 mA, respectively. Data were collected from $2\theta = 10$ to 80° at a scanning rate of 8° min^{-1}. SEM photos were taken using a FEI Quanta 200 SEM, which was fitted with a Peltier-cooled stage during SEM operation. Energy-dispersive X-ray analysis (EDX) was used to obtain a chemical analysis of particular crystals or regions. Before the SEM observations, these samples were mounted in epoxy resin and polished to 1μm with diamond slurries. The mirror surfaces of specimens were sputtered with a platinum coating. High-resolution TEM observations were carried out using a JEM-2100F transmission electron microscope operating at 200 kV.

Table 2. Composition (wt%) of the investigated glass–ceramic Si_3N_4 composites.

	Composition (wt%)			Composition (wt%)	
Sample no.	Glass frit (GY#)	α-Si_3N_4	Sample no.	Glass frit (GL#)	α-Si_3N_4
GY-30	30	70	GL-30	30	70
GY-35	35	65	GL-35	35	65
GY-40	40	60	GL-40	40	60
GY-45	45	55	GL-45	45	55
GY-50	50	50	GL-50	50	50

The flexural strength and Young's modulus were measured on a specimen bar ($4 \times 4 \times 25\,mm^3$ with accuracy ± 0.02 mm) using an electronic multipurpose tester (CSS-44100 model) with a span of 14.5 mm and a crosshead speed of $0.2\,mm\,min^{-1}$. The values for bending strength σ and Young's modulus E were calculated according to the following equations:

$$\sigma = 3FL/(2bh^2), \tag{1}$$

$$E = kL^3/(4bh^3), \tag{2}$$

where F is the load at failure (N), L is the span (mm), b is the sample width (mm), h is the thickness (mm) and k the slope (dF/dv) in the load–deflection curve.

Fracture toughness was determined by the single edge-notched beam method (SENB) with a span of 30 mm, and the size of the specimen was $2.5 \times 5 \times 40\,mm^3$ with an accuracy ± 0.02 mm. Vickers hardness was measured using a microhardness tester (DHV-1000-CCD) with a pyramid-shaped diamond indenter. The specimens' surfaces were polished to a 1μm diamond finish. A load of 2 kg was applied on polished samples.

3. Results and discussion

3.1 *Sintering and phase characterization*

Figure 1 shows the DSC curves of the two glasses (GY# and GL#). The DSC curves of the glass samples GY# and GL# show well-defined glass transition ranges (T_g) and two obvious exothermic peaks (T_c) corresponding to crystallizations of some possible crystalline phases. From the DSC curves in figure 1, two obvious exothermic peaks of both the glass samples GY# and GL# were between 1100 and 1250°C. These

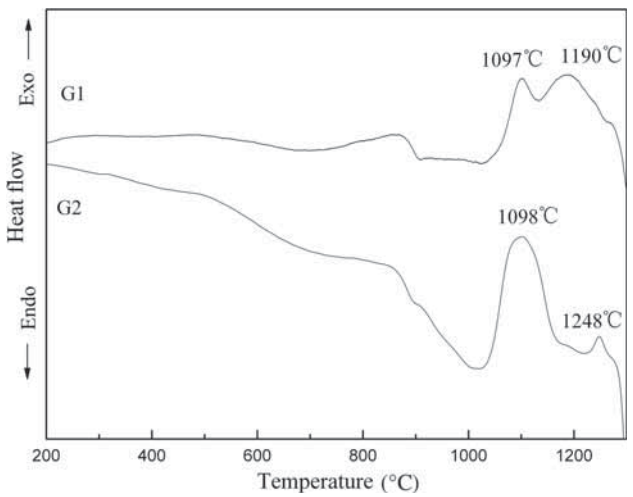

Figure 1. DSC curves of the RE_2O_3–Al_2O_3–SiO_2 glass samples GY# and GL# with a particle size distribution between 48 and 75 μm.

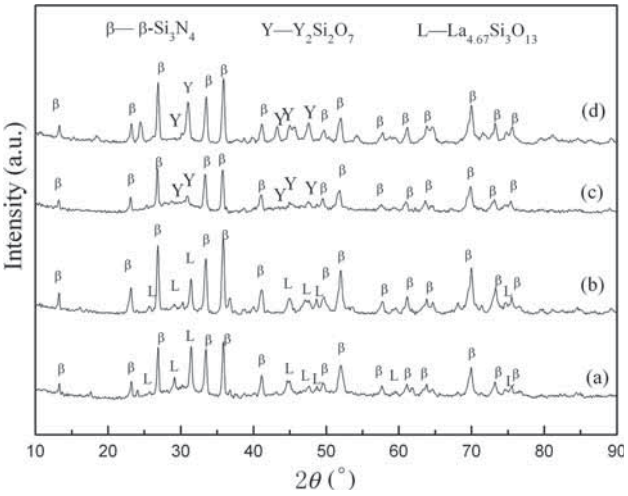

Figure 2. XRD patterns of products of the composite samples after sintering: (**a**) GY-35, (**b**) GY-50, (**c**) GL-35 and (**d**) GL-50.

two glass samples have almost the same first crystallization peak temperature (T_{c1}) at ~1100°C. However, a large difference in the second crystallization peak (T_{c2}) is observed. It is much weaker and located at a higher temperature (~1248°C) for the glass sample GL#. This evidence suggests that the effects of different rare-earth oxides on the crystallization behaviour of the investigated RE_2O_3–Al_2O_3–SiO_2 glasses are different. This suggests that the RE_2O_3–Al_2O_3–SiO_2 glass containing Y_2O_3 tends to crystallize more easily.

After the sintering process, the obtained samples were analysed to identify their crystalline phases by XRD patterns using Jade 6.0. Crystalline peaks corresponding to the different crystalline phases are marked with different symbols. Figure 2a and b shows XRD patterns of products of the composites (GL-50 and GL-35) sintered at 1100°C held for 2 h and at 1650°C held for 4 h, respectively. The crystalline phases of the investigated composites after sintering are $La_{4.67}Si_3O_{13}$ and β-Si_3N_4. Figure 2c and d shows XRD patterns of products of the composite samples (GY-50 and GY-35) sintered at 1100°C for 2 h and 1650°C for 4 h, respectively. The crystalline phases of the investigated composites after sintering are $Y_2Si_2O_7$ and β-Si_3N_4. For the samples GY-50, GY-35, GL-50 and GL-35, only a trace of residual α-Si_3N_4 was detected by XRD, indicating that the α- to β-Si_3N_4 phase transformation is almost complete during sintering. Phase analysis of the Si_3N_4 composites showed that the fraction of α- to β-Si_3N_4 phase increased with increasing amount of the mixed rare-earth aluminosilicate glass frit due to the higher liquid phase during the sintering process. The growth kinetics of β-Si_3N_4 grains in glass–ceramic Si_3N_4 composites containing a liquid phase have been studied by Ye *et al* [31] and Ma *et al* [32]. The α- to β-Si_3N_4 phase transformation occurred after solution of fine α-Si_3N_4 grains and subsequent reprecipitation as β-Si_3N_4 in a liquid phase formed from the sintering additive.

As stated earlier, adding 30–50 wt% glass frit served not only as an effective liquid phase aid for attaining full

densification and promoting the α- to β-Si_3N_4 phase transformation, but also formed RE disilicate crystallized phases remaining as a structural matrix.

3.2 *Microstructural studies*

Microstructural studies were carried out using SEM and HR-TEM. Figure 3a–d shows the SEM backscattered electron images of the composite samples GY-50, GY-35, GL-50 and GL-35, respectively. It is obvious that some of these composite samples possess a typical bimodal microstructure composed of elongated β-Si_3N_4 grains distributed in a fine glass–ceramic matrix. After sintering at 1100°C for 2 h and 1650°C for 4 h, well-defined elongated β-Si_3N_4 grains, crystallized rare-earth disilicate ($Y_2Si_2O_7$ or $La_{4.67}Si_3O_{13}$) and grain boundary phases were observed in these samples. Energy-dispersive spectral analysis (EDS) of the intergranular phase revealed the presence of significant La and Y elements, indicative of the expected $Y_2Si_2O_7$ or $La_{4.67}Si_3O_{13}$ phases.

From the micrographs in figure 3, it is obvious that the presence of mixed rare-earth elements (Y and La) in the grain boundary surrounding β-Si_3N_4 grains yields differences in grain growth anisotropy. For the samples GY-50 and GY-35, the typical bimodal microstructure of glass–ceramic Si_3N_4 composites, dispersed homogeneously in the fine-grained matrix was observed, composed of a few large rod-like β-Si_3N_4 grains having an average diameter of about 0.4–0.6 μm, an average length of about 4–6 μm and aspect ratio (AR) of about 6–8. However, for composite samples GL-50 and GL-35, the rod-like β-Si_3N_4 grains had an average diameter of about 0.3–0.4 μm, an average length of about 3–4 μm and a high AR of about 8–10. Thus, it suggests that, in the Si_3N_4 composite samples with 30–50 wt% glass frit, the larger RE^{3+} cations (La^{3+}) can not only promote crystal refinement but also result in the increase of the ARs compared with Y^{3+} ions. In other words, the tendency of the mean sizes of β-Si_3N_4 grains is to decrease from the samples with added Y_2O_3–Al_2O_3–SiO_2 glass frit to the samples with La_2O_3–Al_2O_3–SiO_2 glass frit. However, the tendency of the mean AR of β-Si_3N_4 shows the opposite tendency.

The explanation for different microstructural evolutions of the RE_2O_3–Al_2O_3–SiO_2–Si_3N_4 composites with different compositions of glass frit (GY# or GL#) is different viscosities of the liquid phase at the temperature of sintering. It is supposed that higher viscosity restrains dissolution of Si_3N_4 grains in the melt with a consequence of lower concentration of ions needed for the precipitation. This result can be attributed to the incorporation of both the rare-earth ions Y^{3+}

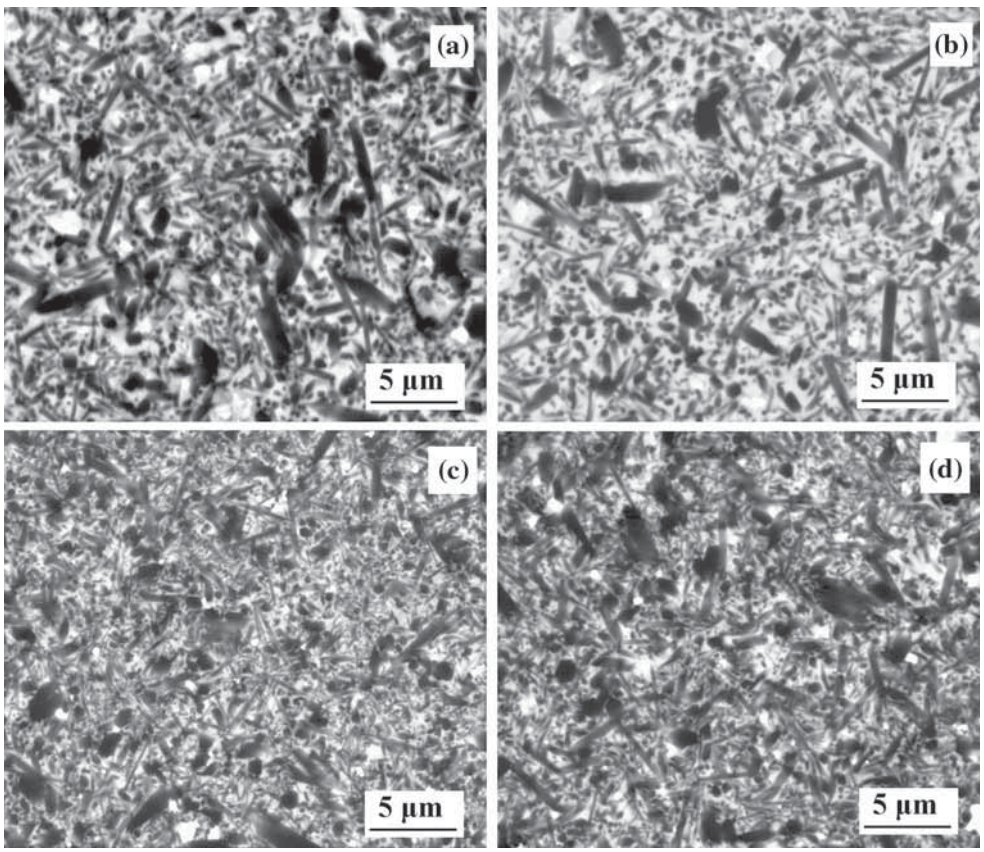

Figure 3. SEM backscattered electron images of the composite samples: (**a**) GY-50, (**b**) GY-35, (**c**) GL-50 and (**d**) GL-35 after sintering at 1100°C for 2 h and 1650°C for 4 h.

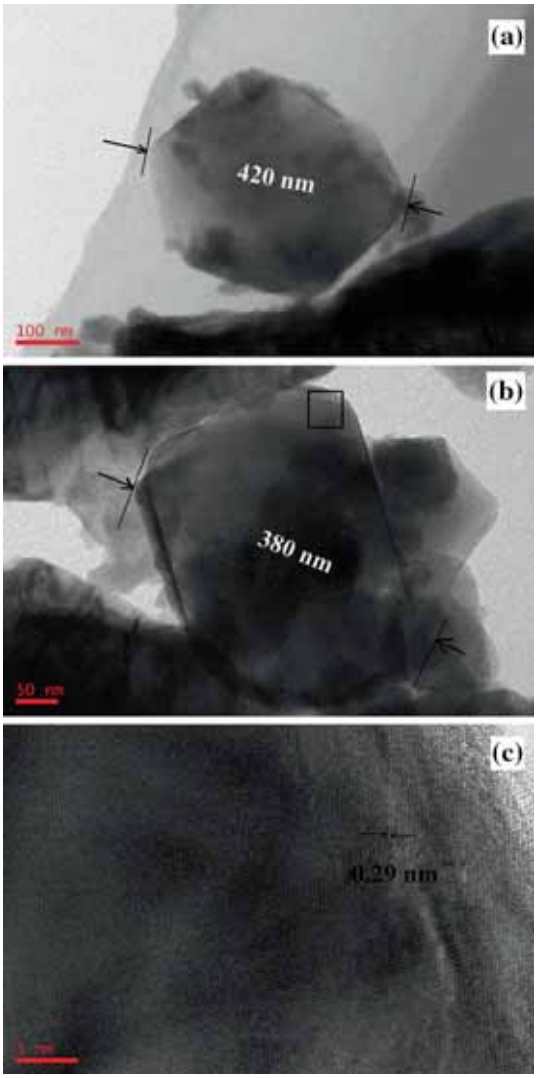

Figure 4. TEM micrograph of the glass–ceramic Si_3N_4 composites: (**a**) GY-35 and (**b**) GL-35 after sintering at 1100°C for 2 h and 1650°C for 4 h; (**c**) HR-TEM analysis of the area enclosed in the black box in **b**.

and La^{3+} into the β-Si_3N_4 lattice. In the present study, the activities of Y and La also play an important role in control of the interface formation. The diffusion of Y and La from the matrix to β-Si_3N_4 grains is attributed to the atomic concentration gradient between the β-Si_3N_4 grains and the RE_2O_3–Al_2O_3–SiO_2 glass–ceramic matrix. This interdiffusion process leads to the formation of a strong interface. Typical TEM micrographs of the composites GY-35 and GL-35 are shown in figure 4a and b, respectively. After sintering at 1200°C for 2 h and 1650°C for 4 h, the prismatic surface of well-defined β-Si_3N_4 whiskers is observed. The 0.29 nm interval of the lattice fringes in prismatic surface is observed in figure 4c.

In general, the β-Si_3N_4 grains are well dispersed in the matrix. The SEM micrographs in figure 3 show a continuous glass–ceramic matrix and randomly dispersed β-Si_3N_4. The difference in grain size of the elongated β-Si_3N_4 grains was remarkable in the different RE_2O_3–Al_2O_3–SiO_2 glass compositions. The large size of the *in-situ* β-Si_3N_4 grains derived from the α-Si_3N_4 precursor in the 50 wt% GY-Si_3N_4 composite was typical for Si_3N_4-reinforced glass–ceramic composites. The randomly dispersed grains in the glass–ceramic composites seem to connect with each other to form a cross-linked network. In this study, a bimodal microstructure could be obtained via a two-step sintering process. During the first-step sintering (1100°C), the crystallization of the RE_2O_3–Al_2O_3–SiO_2 glasses occurred to form rare-earth disilicate crystallized phases. Then at the higher temperature (1650°C) of the second-step sintering process, the residual glass liquid could be formed, which would be beneficial for α-Si_3N_4 to β-Si_3N_4 phase transformation and β-Si_3N_4 grains growth. The liquid RE-containing glassy phase can act as a suitable solvent for Si_3N_4 and assist in α- to β-Si_3N_4 phase transformation.

3.3 *Mechanical properties*

The mechanical properties of the investigated RE_2O_3–Al_2O_3–SiO_2–Si_3N_4 composites are shown in figure 5. The results show that the flexural strength values of the investigated composites are significantly greater than that of non-reinforced rare-earth aluminosilicate glass–ceramics. The flexural strength, Vickers hardness, elastic modulus and fracture toughness of the glass–ceramic Si_3N_4 composites with glass frit GL# reach a maximum of 687 MPa, 14.7 GPa, 224 GPa and 6.9 MPa $m^{1/2}$, respectively. For the glass–ceramic Si_3N_4 composites with glass frit GY#, the flexural strength, Vickers hardness, elastic modulus and fracture toughness reach a maximum of 648 MPa, 13.9 GPa, 216 GPa and 6.4 MPa $m^{1/2}$, respectively. The physical properties of the sintered composite samples GY-35 and GL-35 are shown in table 3.

The fracture surface of the composite sample GY-35 and GL-35 after the flexural strength test is shown in figure 6. The fracture mode is intergranular, indicating the presence of a weak grain boundary that favours crack deflection. Thus, the content of β-Si_3N_4 grains in the composites plays a very vital role in the fracturing process. Moreover, it can be seen that the crack deflection and grain bridging are considered as major toughening mechanisms in this composite. The average flexural strength values of the glass–ceramic Si_3N_4 composites increased greatly compared with the glass–ceramic matrix, indicating that *in-situ*-grown rod-like β-Si_3N_4 grains provided a good strengthening effect by means of the load transfer effect from glass–ceramic matrix to β-Si_3N_4 grains. The flexural strength increased with increasing β-Si_3N_4 content in materials. α-Si_3N_4 is equiaxed and distributed randomly in the glass–ceramic matrix and hence could not serve as an effective reinforcement due to the limited load transfer between the particles and the matrix. On the contrary, β-Si_3N_4 grain has a whisker-like morphology, which is more effective as reinforcement because it enhances the load transfer from the glass–ceramic matrix to β-Si_3N_4 whisker [33,34].

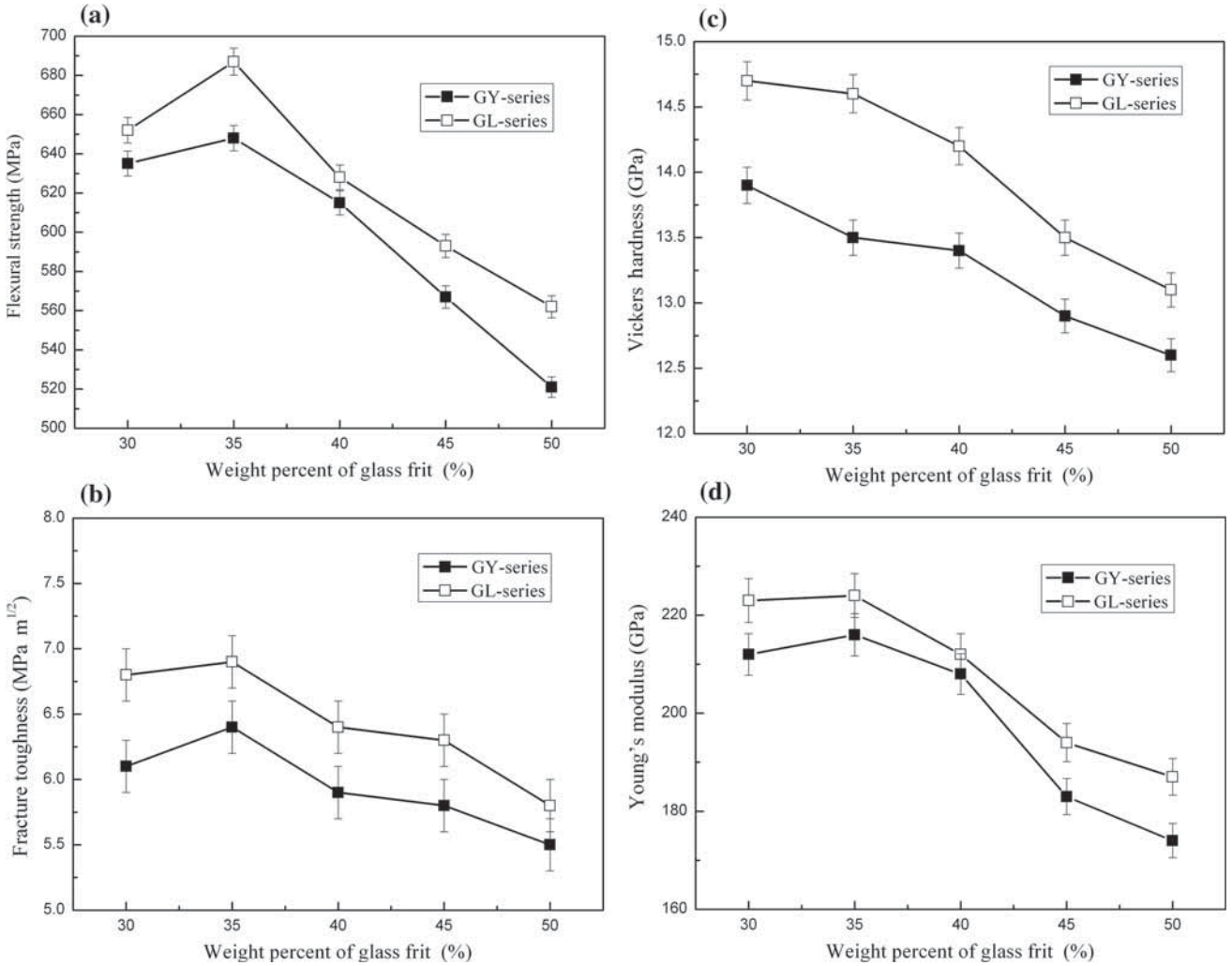

Figure 5. Mechanical properties: (**a**) flexural strength, (**b**) fracture toughness, (**c**) Vickers hardness and (**d**) Young's modulus as a function of the amount of glass frit in the glass–ceramic Si_3N_4 composites for the GY and GL series.

Table 3. The physical properties of the sintered composite samples GY-35 and GL-35.

Properties	GY-30	GL-30
Density (g cm^{-3})	3.26	3.45
Flexural strength (MPa)	648	687
H_V (GPa)	13.9	14.7
K_{1c} (MPa m$^{1/2}$)	6.4	6.9
Elastic modulus (GPa)	216	224

The fracture toughness of the composite materials followed a trend similar to that observed for flexural strength. The 35 wt% GL–Si_3N_4 composites sintered at 1100°C for 2 h and 1650°C for 4 h had the highest content of β-Si_3N_4 and gave the highest toughness (6.9 MPa m$^{1/2}$). However, the fracture toughness of the 50 wt% glass–Si_3N_4 composite was lower than that of the 35 wt% glass–Si_3N_4 composite. The flexural strength and fracture toughness of these composites are also strongly affected by the morphology of β-Si_3N_4 grains, besides its amount. Results for microhardness are also shown in figure 5c. From the microhardness values obtained it can be seen that a decrease in microhardness is observed in the composite samples with 50 wt% glass frit. Both the two composite materials with 35 wt% glass frit after sintering possess higher microhardness values. This may be due to the higher fraction of $\beta/\alpha+\beta$-Si_3N_4. The slight decrease in hardness for the materials with 50 wt% glass slags is attributed to its higher amount of glass addition. Figure 5c shows the clear difference between the GY–Si_3N_4 composite samples and the GL–Si_3N_4 composite samples in microhardness. Figure 5d demonstrates the dependence of Young's modulus on the content of glass frit at room temperature. The microhardness is a valuable mechanical property for ceramics, which is often utilized when an abrasive or grinding action is required. It is seen from figure 5c and d that both the microhardness and Young's modulus of glass–ceramic Si_3N_4 composites decreased with increasing content of glass frit.

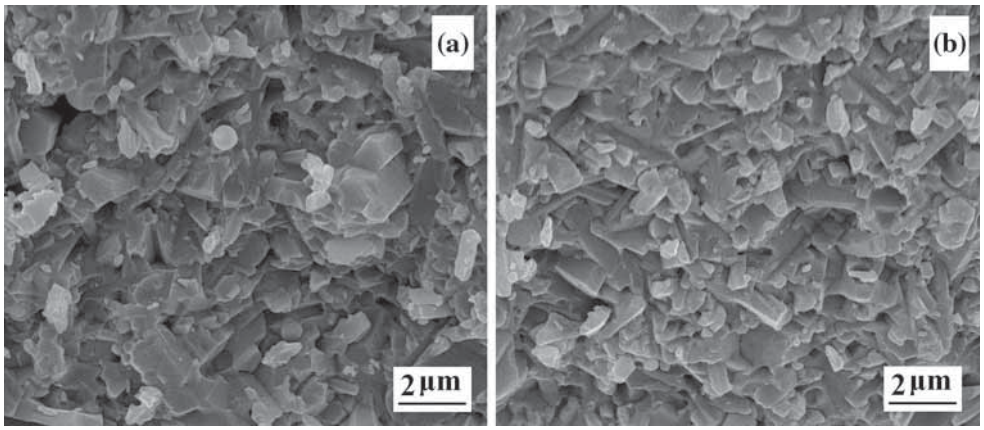

Figure 6. SEM micrographs of the fracture surfaces after flexural strength test of the glass–ceramic Si_3N_4 composites: (**a**) GY-35 and (**b**) GL-35 after sintering at 1100°C for 2 h and 1650°C for 4 h.

It was usually recognized that the flexural strength and fracture toughness of Si_3N_4-based composite materials are dependent on the amount, size and geometry of the elongated β-Si_3N_4 grains, and the properties of grain boundary phases [35]. The addition of 35 wt% glasses results in higher flexural strength and fracture toughness than those with 50 wt% glasses due to their more elongated microstructure and higher content of β-Si_3N_4 phase, and therefore, improved crack deflection and crack-bridging mechanisms. The composite materials with glass frit GL containing La_2O_3 possess higher Vickers hardness than that with the same content of glass frit GY containing Y_2O_3. This is undoubtedly due to the increase in the number of elongated β-Si_3N_4 grains with higher AR. Lai and Tien [36] have found that the relationship between sintering temperature and AR of β-Si_3N_4 can be expressed as the following equation:

$$\ln \mathrm{AR} = \ln\left(\frac{K_L^{1/3}}{K_W^{1/5}}\right) + \frac{2}{15}\ln t - \frac{(Q_L/3 - Q_W/5)}{RT},$$

where Q_L and Q_W are activation energies, and K_L and K_W are rate constants in the length and width directions, respectively.

This anisotropic grain growth behaviour is known to be markedly altered by the addition of some metal oxides, most notably the rare-earth oxides. Thus, selective dopant additions offer the potential for tailoring the mechanical properties through microstructure optimization. La_2O_3 additions are known to strongly promote anisotropic grain growth, resulting in the highest AR grains compared with other rare-earth oxides [19]. Similarly, the enhancement of anisotropic grain growth by glass frit additions containing La_2O_3 must derive from preferential segregation that suppresses diametrical growth involving the prismatic surfaces. Thus, adding glass frit GL containing La_2O_3 can not only promote crystal refinement but also result in the increase of the ARs, as the grain size in width was decreased more than that in length. The improvement of the sinterability of Si_3N_4 with the enhanced homogeneity of the sintering additives distributed over the matrix and the resultant higher relative density are quite easily suggested as partially responsible for the improvement of the mechanical properties [37,38]. Not only the microstructural factors but also the phase composition and chemistry of the secondary phases significantly affect the mechanical properties of these composites.

As stated earlier, a two-step growth mechanism of rare-earth disilicates matrix and elongated β-Si_3N_4 grains is proposed for the growth of the RE_2O_3–Al_2O_3–SiO_2–Si_3N_4 composite materials; crystallized rare-earth disilicate matrix at 1100°C is assumed to restrict the softening of the residual glassy phase at a higher temperature of 1650°C. However, the mechanical properties of all the investigated composite materials are lower than those of the pure Si_3N_4 ceramic reported in the literatures. This can be attributed to a reduction *in-situ* β-Si_3N_4 grain size to a certain extent, a relatively lower sintering temperature (1650°C), a relatively higher residual glassy phase content, etc.

4. Summary

In conclusion, *in-situ*-grown β-Si_3N_4-reinforced RE_2O_3–Al_2O_3–SiO_2 glass–ceramic matrix composites were processed at a relatively lower temperature (1650°C). Moreover, the effects of the composition on the microstructure and properties of the RE_2O_3–Al_2O_3–SiO_2–Si_3N_4 composites were investigated. The conclusions are summarized as follows.

RE_2O_3–Al_2O_3–SiO_2 glasses can serve as an effective aid to promote the densification of Si_3N_4 composites and the α- to β-Si_3N_4 phase transformation. The mechanical properties of the glass–ceramic can be effectively improved by *in-situ*-grown elongated β-Si_3N_4 grains. The flexural strength,

fracture toughness, Young's modulus and Vickers hardness of glass–ceramic Si_3N_4 composites increase greatly compared with the glass–ceramic matrix. During the first-step sintering process, the crystallization of the glasses occurred, resulting in the formation of rare-earth disilicate phases. Then, during the second-step sintering process, the residual glass liquid would be beneficial for the α- to β-Si_3N_4 phase transformation and β-Si_3N_4 grains growth. Adding glass frit containing La_2O_3 can not only promote crystal refinement but also result in the increase in the ARs, as the grain size in width is decreased more than that in length. The crack deflection and grain bridging are considered as major toughening mechanisms in these composites. The crystalline phases of the investigated composites after sintering are $Y_2Si_2O_7$ (or $La_{4.67}Si_3O_{13}$) and β-Si_3N_4. $Y_2Si_2O_7$ can be used in severe environments with high-temperature water vapour corrosion and fast cooling–heating cycle owning to its good damage tolerance and low CTE. These glass–ceramic Si_3N_4 composites with excellent comprehensive properties might be a promising material for high-temperature applications.

Acknowledgements

This research was financially supported by the National Natural Science Foundation of China (Numbers 51502349 and 51272288).

References

[1] Fu F, Chen B, Shen L, Pun E Y B and Lin H 2014 *J. Alloys Compd.* **582** 265
[2] Marchi J, Morais D S, Schneider J, Bressiani J C and Bressiani A H A 2005 *J. Non-Cryst. Solids* **351** 863
[3] Iftekhar S, Grins J and Eden M 2010 *J. Non-Cryst. Solids* **356** 1043
[4] Iftekhar S, Grins J, Gunawidjaja P N and Eden M 2011 *J. Am. Ceram. Soc.* **94** 2429
[5] Lofaj F, Satet R, Hoffmann M J and Arellano-López A R 2004 *J. Eur. Ceram. Soc.* **24** 3377
[6] Leonova E, Hakeem A S, Jansson K, Stevensson B, Shen Z, Grins J *et al* 2008 *J. Non-Cryst. Solids* **354** 49
[7] Wakihara T, Tatami J, Komeya K, Meguro T, Kidari A, Hampshire S *et al* 2012 *J. Eur. Ceram. Soc.* **32** 1157
[8] Redington W, Kidari A, Redington M, Laffir F, Pomeroy M J and Hampshire S 2012 *J. Eur. Ceram. Soc.* **32** 1359
[9] Luo Z, Qu G, Chen X, Liu X and Lu A 2013 *J. Non-Cryst. Solids* **361** 17
[10] Satet R L and Hoffmann J 2004 *J. Eur. Ceram. Soc.* **24** 3437
[11] Pomeroy M J, Nestor E, Ramesh R and Hampshire S 2005 *J. Am. Ceram. Soc.* **88** 875
[12] Li X and Lu A 2011 *Bull. Mater. Sci.* **34** 767
[13] Luo Z, Lu A, Qu G and Lei Y 2013 *J. Non-Cryst. Solids* **362** 207
[14] Hampshire S and Pomeroy M J 2012 *J. Eur. Ceram. Soc.* **32** 1925
[15] Shen Z, Zhao Z, Peng H and Nygren M 2002 *Nature* **417** 266
[16] Lee Y, Kim Y, Choi H and Lee J 2001 *J. Mater. Sci.* **36** 699
[17] Asthana R, Singh M and Martinez-Fernandez J 2013 *J. Alloys Compd.* **552** 137
[18] Go P, Sung C, Kostetsky J J and Vasilos T 2002 *J. Mater. Sci.* **37** 2587
[19] Zhou Y, Hyuga H, Kusano D, Yoshizawa Y and Hirao K A 2011 *Adv. Mater.* **23** 4563
[20] Bal B S and Rahaman M N 2012 *Acta Biomater.* **8** 2889
[21] Ye F, Chen S and Iwasa M 2003 *Scr. Mater.* **48** 1433
[22] Liu L, Ye F, Zhou Y and Zhang Z 2010 *Scr. Mater.* **63** 166
[23] Ye F, Liu L, Zhang J, Iwasa M and Su C 2005 *Compos. Sci. Technol.* **65** 2233
[24] Ye F, Zhang L, Zhang H, Liu L, Liu C and Zhou Y 2009 *Mater. Sci. Eng. A* **527** 287
[25] Chen S, Ye F and Zhou Y 2002 *Ceram. Int.* **28** 51
[26] Baldacim S A, Santos C, Silva O M M and Silva C R M 2004 *Mater. Sci. Eng. A* **367** 312
[27] Zhang Y, Zhang Y, Han J, Zhou Y, Hu L, Yao W *et al* 2008 *Mater. Sci. Eng. A* **497** 383
[28] Biswas K, Rixecker G and Aldinger F 2004 *Mater. Sci. Eng. A* **374** 56
[29] Wang C, Chen M, Wang H, Fan X and Xia H 2016 *J. Eur. Ceram. Soc.* **36** 689
[30] Lange F F, Singhal S C and Kuznicki R C 1977 *J. Am. Ceram. Soc.* **60** 249
[31] Ye F, Liu L, Zhang J and Meng Q 2008 *Compos. Sci. Technol.* **68** 1073
[32] Ma J, Ye F, Liu L and Zhang H 2009 *Mater. Sci. Eng. A* **520** 158
[33] Dai J, Li J, Chen Y, Yang L and Sun G 2003 *Mater. Res. Bull.* **38** 609
[34] Ye F, Liu L, Zhang H and Zhou Y 2008 *Mater. Sci. Eng. A* **488** 352
[35] Xia Y, Zeng Y and Jiang D 2012 *Mater. Des.* **33** 98
[36] Lai K R and Tien T Y 1993 *J. Am. Ceram. Soc.* **76** 91
[37] Lojanová S, Tatarko P, Chlup Z, Hnatko M, Dusza J, Lencés Z *et al* 2010 *J. Eur. Ceram. Soc.* **30** 1931
[38] Liu X, Huang Z, Ge Q, Sun X and Huang L 2005 *J. Eur. Ceram. Soc.* **25** 3353